

Asymmetry of characteristic X-ray peaks obtained by a Si(Li) detector

Claudia Visñovezky^a, Silvina Limandri^a, María Elena Canafoglia^b,
Rita Bonetto^{b,c}, Jorge Trincavelli^{a,c,*}

^a *Facultad de Matemática, Astronomía y Física, Universidad Nacional de Córdoba, Ciudad Universitaria, 5000, Córdoba, Argentina*

^b *Centro de Investigación y Desarrollo en Ciencias Aplicadas Dr. Jorge Ronco, Calle 47 N° 257, 1900 La Plata, Argentina,*

Facultad de Ciencias Exactas y Facultad de Ingeniería de la UNLP, La Plata, Argentina

^c *Consejo Nacional de Investigaciones Científicas y Técnicas de la República Argentina*

Received 11 December 2006; accepted 20 May 2007

Available online 25 May 2007

Abstract

The asymmetry of the characteristic X-ray peaks obtained using a Si(Li) detector is mainly due to incomplete charge collection. Impurities and defects in the crystalline structure of Si can act as “traps” for holes and electrons in their trip toward the detector electrodes. Therefore, the collected charge, and consequently the detected energy, is smaller than the expected one. The global effect is that peaks may present a “tail” toward the low energy side. This phenomenon is more important for low energies (lower than 2.3 keV, in the case of the detector characterized).

In this work, the parameters related to peak asymmetry were studied, allowing a better understanding of the trapping process mentioned above. For this purpose, spectra from mono- and multi-element samples were collected for elements with atomic number between 7 and 20. In order to describe the shape of the characteristic K peaks as a function of its energy, an asymmetric correction to a Gaussian function was proposed. Spectra were obtained by electron probe microanalysis for incidence energies between 5 and 25 keV using an energy dispersive spectrometer equipped with an ultra-thin window Si(Li) detector. It was observed that the area corresponding to the asymmetric correction exhibits an energy dependence similar to that of the mass absorption coefficient of the detector material. In addition, other two spectrometers were used to investigate the dependence of tailing on the detection system. When two spectrometers with the same kind of detector and different pulse processors were compared, peaks were more asymmetric for lower peaking time values. When two different detectors were used, differences were even more important.

© 2007 Elsevier B.V. All rights reserved.

Keywords: Si(Li) detector; Peak asymmetry; Spectral deconvolution; Spectral fitting

1. Introduction

When a photon arrives at a Si(Li) detector a large number of electron-hole pairs is created, which move towards the anode and cathode under the influence of an applied external field. In their paths to the electrodes, these charge carriers can be “trapped” in energy levels between the Si valence and conduction bands caused by crystal impurities and defects. Electrons and holes may be subsequently released by thermal excitation, but their contribution to the output pulse may be

partially lost, depending on “trapping” time. Thus, pulse height decrease will be more important for short processing times. In addition, electrons and holes may recombine at the trapping sites; hence their contribution is certainly lost in this case.

The effect of the process of charge trapping on the detected X-ray spectrum is observed as an asymmetric tail at the low energy side of characteristic peaks, since less charge than expected may be collected and therefore the respective pulse will be decreased, and the assigned energy will be correspondingly lower. In the front face of a Si(Li) detector there is a first region not effective for detection, known as dead layer. Between the active region and the dead layer there is a partially active zone, where a great number of trapping sites is present; thus, if the incident characteristic photons are efficiently absorbed there, most of the charge carriers will be produced in this region [1].

* Corresponding author. Facultad de Matemática, Astronomía y Física, Universidad Nacional de Córdoba, Ciudad Universitaria, 5000, Córdoba, Argentina.

E-mail addresses: cavy3@hotmail.com (C. Visñovezky), silvilimandri@hotmail.com (S. Limandri), bonetto@quimica.unlp.edu.ar (R. Bonetto), jorge@quechua.fis.uncor.edu (J. Trincavelli).

When the electron-hole pairs are generated within the full active region of the detector (almost free of trapping sites), electrons will move to the anode, whereas holes will go to the cathode, through the partially active layer, with a high probability of trapping. The trapping of holes almost does not affect the height of the collected pulse because it is mainly formed by the electrons (their mobility within the semiconductor is around two times the hole mobility). On the other hand, when the charge carriers are originated in the partially active layer, both holes and electrons must traverse it with high probability of trapping. In this case, the pulse collected is lower than expected. This fact causes the assignation of an energy value to each incident characteristic photon lower than its true value, contributing to the low energy tail observed in the characteristic peak.

The aim of the present work is to develop a method to model the asymmetry of characteristic peaks for a given spectrometer. To this purpose, X-ray spectra from pure and compound standards containing elements of the third period were collected. The K characteristic lines emitted by these elements cover the energy region where peak asymmetry is appreciable for the detection system analyzed.

A good knowledge of the dependence of asymmetry parameters on the photon energy is necessary to improve the quality of spectral deconvolution or fitting in samples with strong peak overlapping and to obtain more accurate quantitative analysis.

It is known [2,3] that the low energy tail may depend on the detector and also on the electronics associated to it. In order to study the dependence of tailing on the spectrometer, additional spectra were measured with three different instruments.

2. Experimental

With the purpose of characterizing the asymmetric behavior of the detected peaks, X-ray spectra from mineral (anhydrite: CaSO_4 , tugtupite: $\text{Na}_4\text{BeAlSi}_4\text{O}_{12}\text{Cl}$, apatite: $\text{Ca}_5(\text{PO}_4)_3(\text{OH})$, diopside: $\text{MgCaSi}_2\text{O}_6$, dolomite: $\text{MgCa}(\text{CO}_3)_2$ and magnesium nitrate) and pure (Al, Si and Mg) standards were measured at incidence energies between 5 and 25 keV, with beam currents between 0.013 and 1.89 nA, resulting in dead time values between 0.6% and 12%.

Different spectrometers were used to investigate the influence of the detection system on peak asymmetry: a detector with ultra-thin window at the Centro de Investigación y Desarrollo en Ciencias Aplicadas Dr. Jorge Ronco, La Plata, Argentina (system 1); the same kind of detector with a different pulse processor at the Laboratorio de Microscopía Electrónica y Microanálisis, Universidad de San Luis, Argentina (system 2) and a detector with beryllium window at the Universidade Federal de Rio Grande do Sul, Porto Alegre, Brazil (system 3). The main technique specifications of them are the following:

2.1. System 1

The energy dispersive spectrometer EDAX Prime DX4 is attached to a scanning electron microscope Philips SEM 505.

The corresponding detector is a Si(Li) SUTW Sapphire with ultra-thin polymer window and aluminium ohmic contact. The dead layer thickness estimated is 85 nm.

The ultra-thin window is a Moxtek AP3.3 consisting of a 38 μm thick silicon support structure with 77% open area. The window itself is composed of:

Polymer: 300 nm thick, density 1.4 g/cm^3 (69% C, 3% H, 21% O, 7% N)

Aluminium: 30 nm thick, density 2.7 g/cm^3

Boron hydride: 20 nm thick, density 2.0 g/cm^3 (92% B, 8% H)

The EDAX 187 amplifier included in this spectrometer produces a triangular pulse output with a step input from the preamplifier. This triangular filter is a pole-zero variant of a Gaussian filter. The peaking time was set to 70 μs and the analog-to-digital converter (ADC) is Wilkinson type.

2.2. System 2

The energy dispersive spectrometer EDS Genesis 2000 is attached to a scanning electron microscope LEO 1450 VP. The Si(Li) detector is identical to the one of system 1.

This system involves a digital pulse processor and the selected peaking time was 51.2 μs .

2.3. System 3

The electron microprobe CAMECA SX-50 is equipped with a Si(Li) detector with beryllium window (9.2 μm thick) and gold ohmic contact (19 nm thick). The dead layer thickness is estimated to be 280 nm.

3. Spectrum prediction

A method for refining atomic and experimental parameters developed for electron probe microanalysis (EPMA) was used for spectral processing. This method consists in minimizing the differences between an experimental spectrum and an analytical function proposed to predict it. This function takes into account characteristic peaks, bremsstrahlung and different detection artifacts. Thus, the quantity to be minimized is:

$$\chi^2 = \frac{1}{N - P} \sum_i \frac{(\tilde{I}_i - I_i)^2}{I_i}$$

where N is the number of channels in the spectrum, P is the number of parameters fitted, \tilde{I}_i and I_i are respectively the predicted and experimental intensities for the energy E_i of channel i .

This procedure, known in the field of X-ray diffraction as the Rietveld method [4–6], was previously used in EPMA for detector characterization [7] and for the determination of relative transition rates for K [8] and L [9] lines in elements of several atomic number and under different experimental conditions. The algorithm, implemented in the software POEMA [7], starts from certain initial values for the different

parameters involved, which are optimized by means of a numerical iterative process. To get good results, the minimization algorithm must be robust and reliable, and, on the other hand, the model used to describe the whole spectrum I_i must take properly into account characteristic peaks $P_{j,q}$ and bremsstrahlung B as well as detection features:

$$\tilde{I}_i = B(E_i) + \sum_{j,q} P_{j,q} H_{j,q}(E_i) + D(E_i)$$

where $E_i = \text{zero} + i \cdot \text{gain}$ is the energy corresponding to channel i , $H_{j,q}$ is a modified Gaussian function (see below) associated with the peak intensity, and the function D takes into account the contribution of escape peaks, sum peaks and the Si peak generated within the detector. The expressions used for $B(E_i)$ and $P_{j,q}$ involve corresponding scaling factors, which are parameters to optimize. In addition, other parameters refined in the present work were the zero and the gain of the detection chain and the peak-width factors (noise and Fano factor) [7].

In the algorithm used, an asymmetric correction to a Gaussian function was proposed to adequately describe the characteristic peaks. This correction is based on the Hypermet function [10], where the term corresponding to the Heaviside step function was removed, since this behavior is already taken into account by the absorption edges related to the mass absorption photoelectric coefficients. The expression used to describe the characteristic peaks result to:

$$H_{j,q}(E_i) = M[G_{j,q}(E_i) + T_{j,q}(E_i)]$$

where M is a normalization factor defined so as the integral of $H_{j,q}(E_i)$ be equal to unity, $G_{j,q}(E_i)$ is a Gaussian function of width $\sigma_{j,q}$, centered at the characteristic energy $E_{j,q}$ of the line q of element j and $T_{j,q}(E_i)$ is an exponential tail convoluted with a Gaussian and characterized by two parameters, the width $\beta_{j,q}$ and the high $t_{j,q}$ (refined in the optimization process):

$$T_{j,q}(E_i) = t_{j,q} e^{(E_i - E_{j,q})/\beta_{j,q}} \operatorname{erfc} \left(\frac{E_i - E_{j,q}}{\sqrt{2}\sigma_{j,q}} + \frac{\sigma_{j,q}}{\sqrt{2}\beta_{j,q}} \right) \quad (1)$$

The contribution of the function $T_{j,q}$ to the total peak area, which takes into account the incomplete charge collection, can be seen in Fig. 1.

To estimate the uncertainties of the optimized parameters the intensities registered in each spectral channel are considered as stochastic variables obeying Poisson statistics, i.e., their standard deviation is given by the square root of their mean value. The errors related to the refined parameters are then obtained from error propagation of the intensity of each channel by means of numerical derivation [11].

4. Results and discussion

The strategy of optimization was similar for all the spectra analyzed. As an example, the steps given to optimize the Na K α line in a tugtupite sample (see whole spectrum in Fig. 2a) are detailed as follows. In a first step, the bremsstrahlung scale factor, zero and gain were refined using a large spectral region

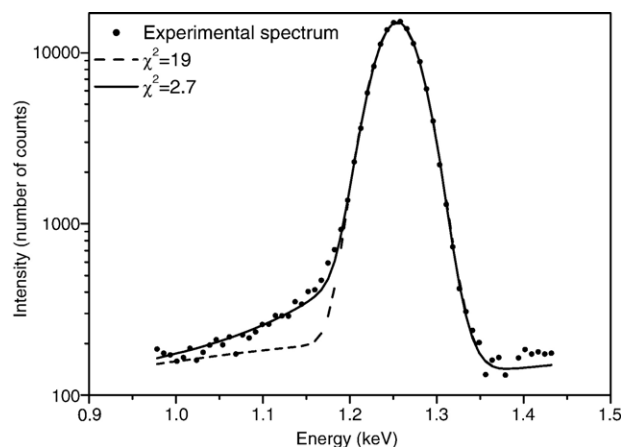


Fig. 1. Spectral region corresponding to the characteristic Mg K α line. The fitting obtained by using a Gaussian distribution for the peak is shown (dashed line) as well as the fitting resulting by using the function which involves the asymmetry due to incomplete charge collection (continuous line).

(0.36–4.00 keV as can be seen in Fig. 2b). In the next step, the peak scale factor was refined and then, the peak-width factors were added. As can be seen, the logarithmic scale emphasizes the disagreement around O K α and Na K α peaks. This discrepancy arises since at the beginning of the optimization process, the asymmetry parameter t in Eq. (1) is set to zero. Later on, the peak scale factor and noise were optimized again for a reduced region (50 to 100 channels around the considered peak, depending on its width), leaving the bremsstrahlung scale parameter, Fano factor, gain and zero fixed (the last parameter was refined again for certain exceptional cases). Finally, the asymmetry parameters β and t were refined in the same reduced spectral region. This spectrum presents an additional complication, because the Cl K α escape peak appears close to the low energy tail of the Na K α line. Nevertheless, as the algorithm takes into account escape peaks according to the expression proposed by Statham [12], a good fit is obtained (Fig. 2c). The selected interval is very important, since if the spectral region used to optimize bremsstrahlung is too small, the continuum could increase at expenses of the peak asymmetry. The asymmetry parameters, instead, are fitted in a region close to the considered line, because they strongly depend on energy, so that each peak must be studied separately.

4.1. Dependency of peak asymmetry on dead time and incidence energy

The first analysis performed for peak asymmetry was intended to study its possible dependence on the detection dead time DT. To this end, Si pure spectra were measured at different beam currents, and hence, with different DT values. It was verified that the effect of incomplete charge collection does not depend on the saturation level of the detector within the DT range considered. In fact, as it is shown in Fig. 3, the values fitted for the area $A_{j,q}$ arising from the asymmetric correction for different values of dead time, result indistinguishable considering the corresponding uncertainties. The parameter plotted

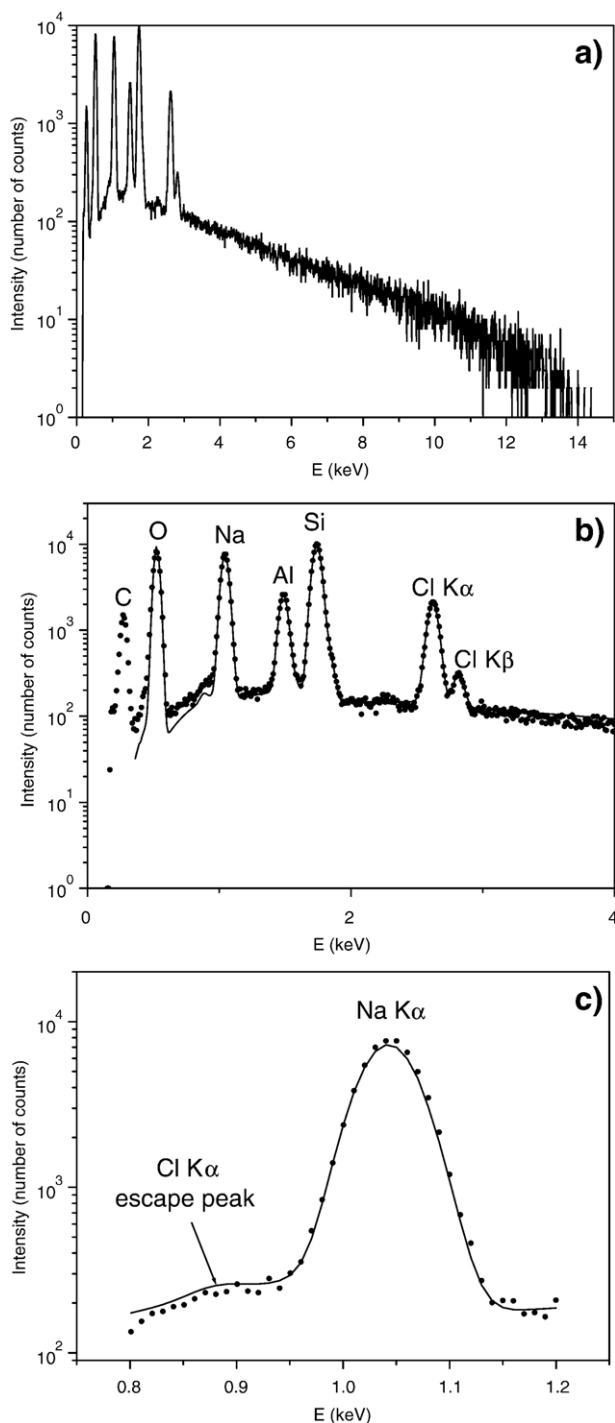


Fig. 2. Tugtupite spectrum; dots: experimental data, solid line: fit curve. a) Whole spectrum. b) Bremsstrahlung, peak, calibration and noise parameters were refined in a large spectral region ($\chi^2=9$). c) Refinement of the asymmetry parameters for the Na K α line in a narrower region ($\chi^2=3$).

represents the fractional area of the asymmetric tailing and is defined as the integral of the function $T_{j,q}$:

$$A_{j,q} = M \int_0^\infty dE_i t_{j,q} e^{(E_i - E_{j,q})/\beta_{j,q}} \operatorname{erfc} \left(\frac{E_i - E_{j,q}}{\sqrt{2}\sigma_{j,q}} + \frac{\sigma_{j,q}}{\sqrt{2}\beta_{j,q}} \right) \quad (2)$$

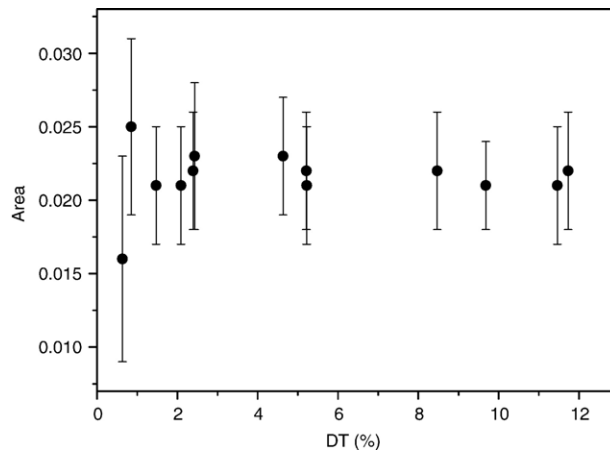


Fig. 3. Area of the asymmetric correction as a function of dead time for silicon pure spectra. The error bars correspond to one standard deviation.

The uncertainties of $A_{j,q}$ plotted in Figs. 3 and 4 were estimated by error propagation of $\beta_{j,q}$ and $t_{j,q}$, from Eq. (2). On the other hand, the possible dependence of asymmetry on the energy E_0 of the incident electron beam was investigated. To this purpose, each sample was measured at different E_0 values. In this case, as in the previous one, no dependence was found, which can be seen exemplified for silicon in Fig. 4.

4.2. Dependency of peak asymmetry on characteristic energy

The next step was to study the dependence of asymmetry on photon characteristic energy. To this end, several spectra were measured for each sample at different E_0 and beam current values. As shown above, this strategy is equivalent to repeat spectra, improving statistics, since no dependence of asymmetry was found on E_0 and DT. It was observed that the parameters $\beta_{j,q}$ and $t_{j,q}$ are strongly correlated in the region of low energies, especially for oxygen.

This means that even when each of these parameters shows a large dispersion (around 300%), the corresponding values for

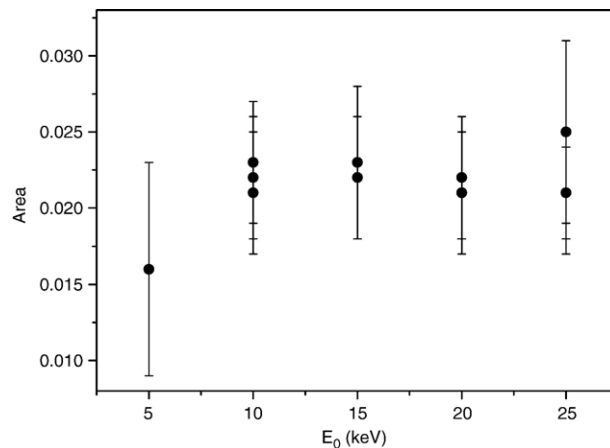


Fig. 4. Area of the asymmetric correction as a function of the incident electron energy E_0 for a silicon pure sample. The error bars correspond to one standard deviation.

Table 1

Parameters t and β related to peak asymmetry for the O K α peak in a diopside sample

t	β	A
0.48 ± 0.02	0.12 ± 0.05	0.11 ± 0.04
0.53 ± 0.19	0.11 ± 0.04	0.11 ± 0.06
0.67 ± 0.22	0.09 ± 0.03	0.12 ± 0.05
0.21 ± 0.07	0.25 ± 0.18	0.09 ± 0.06

In the third column, the corresponding value for the asymmetric area is shown. The uncertainty intervals correspond to one standard deviation.

the asymmetric area $A_{j,q}$ are much closer among themselves (dispersion of around 30%), as can be seen in Table 1 for the O–K α peak in a diopside sample at different experimental conditions. For higher energy peaks, this strong correlation was not observed.

Although the parameters fitted are $\beta_{j,q}$ and $t_{j,q}$, the meaningful quantity is $A_{j,q}$ since it gives a measure of the peak asymmetry. Therefore, bearing in mind the strong correlation found between $\beta_{j,q}$ and $t_{j,q}$ in certain cases, and due to the greater uncertainty of $\beta_{j,q}$ (see Table 1), the following strategy was applied: $\beta_{j,q}$ was obtained from Eq. (2) imposing that along with the average value $\langle t_{j,q} \rangle$, the average value $\langle A_{j,q} \rangle$ is obtained, where averages are taken over all the spectra containing the line q of element j . Regarding the estimation of errors (σ), for the values of $\langle t_{j,q} \rangle$ and $\beta_{j,q}$ presented in Table 2, error propagation was performed iteratively, starting from an initial value $\sigma_\beta = 0$ whereas for $\langle A_{j,q} \rangle$ the statistical deviation was considered. For the particular case of nitrogen, this strategy could not be used, since the iterations diverge; for this reason, the statistical deviation was considered for $\langle t_{j,q} \rangle$ and $\langle A_{j,q} \rangle$, and the error of $\beta_{j,q}$ was obtained by propagation. In Table 2, the values obtained for $\langle t_{j,q} \rangle$, $\beta_{j,q}$ and $\langle A_{j,q} \rangle$ are shown for the characteristic energies of the elements studied.

In Fig. 5, the asymmetric area as a function of characteristic energy is plotted along with the mass absorption coefficient (μ) of silicon, calculated with the software XCOM [13]. Both variables exhibit a similar behavior, which can be explained for the high concentration of trapping sites in the partially active region of the detector: the higher the attenuation coefficient, the higher the probability of photon absorption in the first region, and hence, of incomplete charge collection.

Table 2

Asymmetry parameters $\langle t_{j,q} \rangle$ and $\beta_{j,q}$ for the characteristic K α energies of the analyzed elements

E (keV)	$\langle t_{j,q} \rangle$	$\beta_{j,q}$	$\langle A_{j,q} \rangle$
0.392	0.495 ± 0.005	0.56 ± 0.01	0.28 ± 0.01
0.525	0.51 ± 0.03	0.094 ± 0.05	0.093 ± 0.014
1.041	0.147 ± 0.014	0.19 ± 0.03	0.056 ± 0.005
1.254	0.111 ± 0.008	0.13 ± 0.02	0.028 ± 0.02
1.487	0.079 ± 0.007	0.16 ± 0.02	0.024 ± 0.002
1.740	0.048 ± 0.005	0.23 ± 0.03	0.022 ± 0.002
2.013	0.13 ± 0.02	0.21 ± 0.03	0.054 ± 0.006
2.308	0.033 ± 0.003	0.94 ± 0.11	0.057 ± 0.004

In the last column, the asymmetric area $\langle A_{j,q} \rangle$ averaged over several spectra measured for each sample under different experimental conditions can be observed. The uncertainty intervals correspond to one standard deviation.

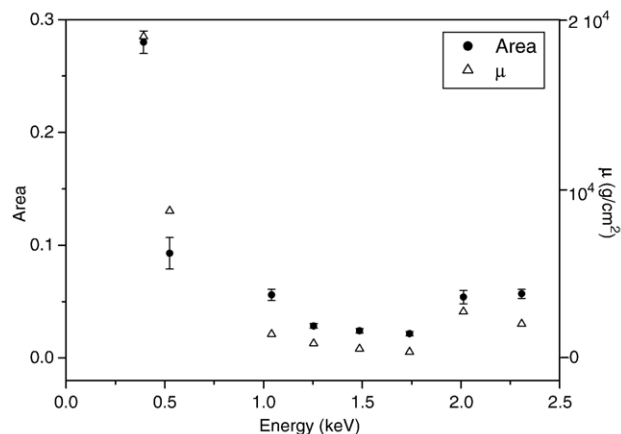


Fig. 5. Asymmetric area and mass absorption coefficient of silicon as a function of characteristic energy. The error bars correspond to one standard deviation.

The asymmetric area decreases with energy, up to the energy corresponding to the silicon absorption edge, showing a similar trend to that followed by μ . The effect of peak asymmetry was not observed for energies greater than 2.3 keV with the detector used. In fact, for greater energies, peaks become more symmetric and they may be properly described by a pure Gaussian function.

4.3. Comparison with other spectrometers

All the results presented above were obtained with system 1. In order to study the dependence of tailing on the detection system, spectra measured with the same kind of detector and different pulse processors are compared in Figs. 6 and 7. These figures show Ca spectra from a diopside sample measured with systems 1 and 2, respectively.

As stated above, for system 1, characteristic peaks may be described by Gaussian functions (no asymmetry) for energies greater than 2.3 keV. For the case of system 2, instead, a slight asymmetry is observed at the Ca K α peak (3.69 keV), which causes a decrease in the χ^2 value when this effect is taken into

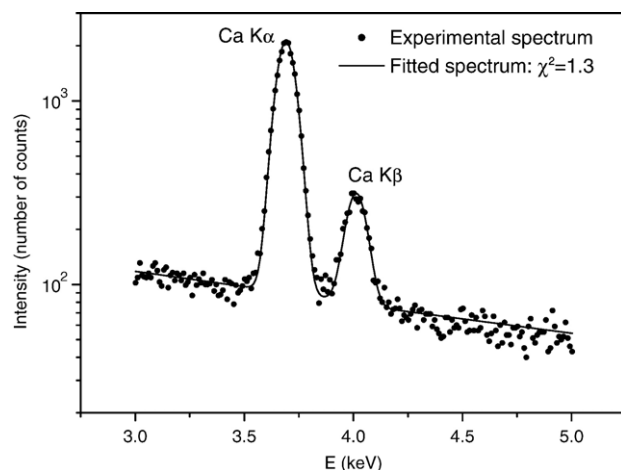


Fig. 6. Ca K lines from a spectrum of a diopside sample measured with system 1. Peaks are symmetric and can be properly fitted by Gaussian functions.

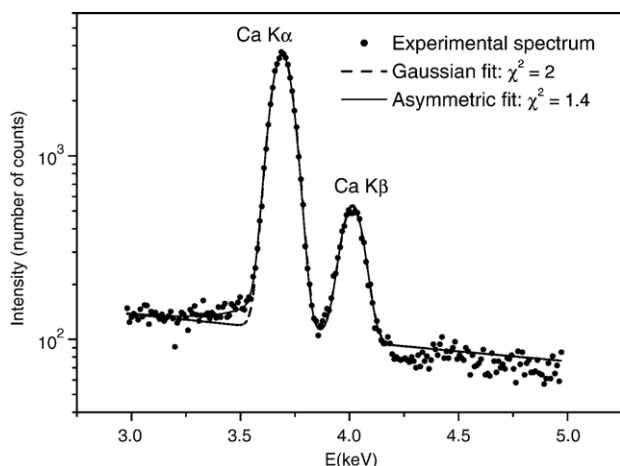


Fig. 7. Ca K lines from a spectrum of a diopside sample measured with system 2. The Ca K α peak exhibits a slight asymmetry.

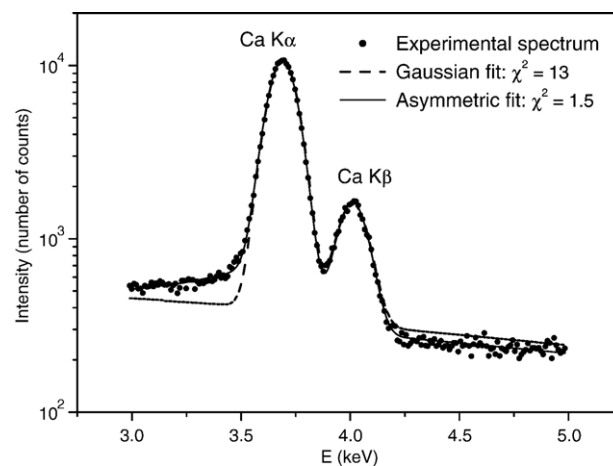


Fig. 8. Ca K lines from a spectrum of a dolomite sample measured with system 3. The Ca K α peak exhibits a strong asymmetry.

account, as shown in Fig. 7. These results evidence that the low energy tail may depend not only on the detector itself but also on the electronics associated to it, which is in agreement with previous work [2,3]. This difference arises from the different peaking times for both pulse processors. For spectrometer 1, the peaking time of the amplifier was set to 70 μ s, whereas for the digital processor of system 2, this value was set to 51.2 μ s. The total processing time for each pulse is, in the first case, $2 \times 70 \mu\text{s} + \sim 40 \mu\text{s} = 180 \mu\text{s}$. In the second case, the whole processing time is $2 \times 51.2 \mu\text{s} + 10 \mu\text{s} = 112.4 \mu\text{s}$. The values for the asymmetry parameters are shown in Table 3; a zero value for parameter t indicates a symmetric peak and in this case parameter β is meaningless (see Eq. (2)). The asymmetry observed for spectrometer 2 may be explained bearing in mind that for short peaking times, charge carriers trapped may not be counted, even if they are released, since they could be detrapped after the pulse is processed. Table 3 also shows the values for the asymmetry parameters corresponding to the Ca K α peak from a dolomite spectrum measured with a different detector (system 3). When the detector is changed (kind of window, ohmic contact, dead layer thickness), differences are still more important (see Fig. 8). Taking into account that the dead layer of the detector in system 3 is much thicker than the one of system 1, it is reasonable to assume that the partially active layer is also thicker in the first detector. This fact explains the stronger asymmetry found for system 3. Another possible cause of the different asymmetry obtained with both detectors could arise from the different ohmic contact

Table 3
Comparison of the asymmetry parameters t , β and A for the Ca K α peak measured in three different spectrometers

System	t	β	A	Peaking time (μ s)
1	0	–	0	70
2	0.323 ± 0.034	0.101 ± 0.033	0.06 ± 0.02	51.2
3	0.132 ± 0.006	0.51 ± 0.02	0.132 ± 0.008	–

The peaking time is given for the pulse processors attached to the first two systems, equipped with identical detectors. The uncertainty intervals correspond to one standard deviation.

materials: gold for system 3 and aluminium for system 1. In the first case, it is possible that atoms of gold migrate to deep regions in the crystal, particularly due to the electric field applied during the detector polarization. It is known that gold impurities occupying substitutional lattice positions of Si, introduce energy levels near the middle of the forbidden gap that can act as traps for charge carriers [14]. On the other hand, in the case of system 1, aluminium has three valence electrons, constituting an acceptor impurity, similar to boron. This last kind of impurities is compensated by the diffused lithium; thus, there is no contribution to peak asymmetry.

5. Conclusion

A method to correct characteristic peak areas between 0.39 and 2.3 keV considering the asymmetric tail towards low energies was developed for a Si(Li) detector with an ultra-thin polymer window. The asymmetric behavior strongly depends on the partially active region of the detector. For the detector characterized, peaks become symmetric for photon energies greater than 2.3 keV.

On the other hand, a dependence of the asymmetry parameters on the pulse processor was also found. Two different pulse processors attached to the same kind of detector (Si(Li) Sapphire) were used and more asymmetric peaks were obtained for lower peaking time values. This fact may be explained bearing in mind that for low peaking time values, charge carriers trapped may not be counted.

When a different detector was used, differences were even more important. The detector with a thicker dead layer, probably accompanied by a thicker partially active layer, produced a stronger asymmetry. The influence of the ohmic contact material on the asymmetry parameters is an issue which should be investigated in detail.

It was observed that the area corresponding to the asymmetric correction behaves similarly as the mass absorption coefficient of the detector material (silicon in the present case). This fact was expected since for higher values of μ , the photons will be probably collected in the front region of the detector,

where the high concentration of trapping sites ensures a poor charge collection.

The present study shows that the function proposed in Eq. (2) describes adequately the characteristic peak shape, taking into account incomplete charge collection. Even when the values found for the parameters $t_{j,q}$ and $\beta_{j,q}$ are specific of one particular Si(Li) detector, it is straightforward to obtain these parameters for other detectors by following the procedure presented here. In addition, it is possible to interpolate $t_{j,q}$ and $\beta_{j,q}$ values for energies not analyzed, provided they are within the range studied.

Since the parameters of asymmetry depend only on photon energy and not on the considered element, these values can be used for L and M lines of heavier elements whose characteristic energies are close to the analyzed ones.

Acknowledgements

The authors wish to thank Dr. Alejo Carreras and Prof. Marcos Vasconcellos for their assistance in the measurement of some of the spectra used for this work.

This work was partially supported by the Consejo Nacional de Investigaciones Científicas y Técnicas de la República Argentina, the Agencia Córdoba Ciencia and the Secretaría de Ciencia y Técnica de la Universidad Nacional de Córdoba, Argentina.

References

- [1] S.J.B. Reed, *Electron Microbeam Analysis*, Cambridge University Press, Cambridge, 1975, pp. 140–141.
- [2] T. Papp, On the response function of solid-state detectors, based on energetic electron transport processes, *X-ray Spectrom.* 32 (2003) 458–469.
- [3] T. Papp, A. Papp, J. Maxwell, Quality assurance challenges in X-ray emission based analyses, the advantage of digital signal processing, *Anal. Sci.* 21 (2005) 737–745.
- [4] H. Rietveld, The crystal structure of some alkaline earth metal urates of the type M_3UO_6 , *Acta Crystallogr.* 20 (1966) 508–513.
- [5] H. Rietveld, Line profiles of neutron powder-diffraction peaks for structure refinement, *Acta Crystallogr.* 22 (1967) 151–152.
- [6] H. Rietveld, A profile refinement method for nuclear and magnetic structures, *J. Appl. Crystallogr.* 2 (1969) 65–71.
- [7] R. Bonetto, G. Castellano, J. Trincavelli, Optimization of parameters in electron probe microanalysis, *X-ray Spectrom.* 30 (2001) 313–319.
- [8] G. Castellano, R. Bonetto, J. Trincavelli, M. Vasconcellos, C. Campos, Optimization of K-shell intensity ratios in electron probe microanalysis, *X-ray Spectrom.* 31 (2002) 184–187.
- [9] J. Trincavelli, G. Castellano, R. Bonetto, L-shell transition rates for Ba, Ta, W, Pt, Pb and Bi using electron microprobe, *Spectrochim. Acta Part B* 57 (2002) 919–928.
- [10] G.W. Phillips, K.W. Marlow, Automatic analysis of gamma-ray spectra from germanium detectors, *Nucl. Instrum. Methods Phys. Res.* 137 (1976) 525–536.
- [11] R. Bonetto, A. Carreras, J. Trincavelli, G. Castellano, L-shell radiative transition rates by selective synchrotron ionization, *J. Phys. B: At., Mol. Opt. Phys.* 37 (2004) 1477–1488.
- [12] V.D. Scott, G. Love, S.J.B. Reed, *Quantitative Electron-Probe Microanalysis*, 2nd ed., Ellis Horwood, London, 1995, p. 78.
- [13] <http://physics.nist.gov/PhysRefData/Xcom/Text/download.html>.
- [14] G.F. Knoll, *Radiation Detection and Measurement*, 2nd ed., John Wiley and Sons, New York, 1989, pp. 347–348.